Molecular Psychiatry (2017) 00, 1–9

www.nature.com/mp

ORIGINAL ARTICLE

Genetic Otx2 mis-localization delays critical period plasticity across brain regions

HHC Lee[1,6], C Bernard[2,6], Z Ye[3,6], D Acampora[4,5], A Simeone[4,5], A Prochiantz[2], AA Di Nardo[2] and TK Hensch[1,3]

Accumulation of non-cell autonomous Otx2 homeoprotein in postnatal mouse visual cortex (V1) has been implicated in both the onset and closure of critical period (CP) plasticity. Here, we show that a genetic point mutation in the glycosaminoglycan recognition motif of Otx2 broadly delays the maturation of pivotal parvalbumin-positive (PV+) interneurons not only in V1 but also in the primary auditory (A1) and medial prefrontal cortex (mPFC). Consequently, not only visual, but also auditory plasticity is delayed, including the experience-dependent expansion of tonotopic maps in A1 and the acquisition of acoustic preferences in mPFC, which mitigates anxious behavior. In addition, Otx2 mis-localization leads to dynamic turnover of selected perineuronal net (PNN) components well beyond the normal CP in V1 and mPFC. These findings reveal widespread actions of Otx2 signaling in the postnatal cortex controlling the maturational trajectory across modalities. Disrupted PV+ network function and deficits in PNN integrity are implicated in a variety of psychiatric illnesses, suggesting a potential global role for Otx2 function in establishing mental health.

Molecular Psychiatry advance online publication, 14 February 2017; doi:10.1038/mp.2017.1

INTRODUCTION

Critical periods (CP) of brain plasticity correspond to defined developmental stages during which experience can shape neural circuitry.[1] For example, during these windows in primary visual cortex (V1), acuity and binocularity can be weakened by discordant sensory experience through the two eyes, such as monocular deprivation (MD).[2,3] In humans, such conditions known as 'lazy eye' or amblyopia (blunted vision), occur in 2–4% of the population, currently with no cure beyond age 8.[4] Later, imbalanced visual input typically has little influence on acuity, reflecting the maturational state of fast-spiking, parvalbumin-positive (PV+) inhibitory interneurons.[1,5] A broader role for GABAergic development, and PV+ circuitry in particular, has been implicated in cognitive dysfunction.[6–8] Prenatal stress[9] or neonatal hypoxia[10] can also weaken these vulnerable GABAergic neurons. Mistiming of CP plasticity following genetic or environmental insults may contribute to the etiology of subsequent disorders such as schizophrenia and autism.[11,12]

During postnatal brain development, distinct CPs across different modalities must be well orchestrated. For example, CPs for sensory processing normally arise before more complex, highly integrated cognitive functions.[1] Interestingly, PV+ cells emerge in cortical regions just ahead of their respective CP onset.[13] We have previously shown that the non-cell autonomous homeoprotein Otx2 (orthodenticle homeobox 2) is essential for this PV+ cell maturation in V1 and consequently responsible for regulating CP timing therein.[14,15] Although Otx2 protein has also been found in other cortical regions,[16] a similar developmental role for Otx2 in other modalities beyond V1 remains unknown. Indeed, an *Otx2* polymorphism has been related to bipolar disorder,[17] suggesting a more global role for Otx2. Here, we directly address this question by genetic disruption of a pivotal aspect of postnatal Otx2 signaling.

Plasticity in V1 is controlled by the experience-dependent transfer of Otx2 produced outside the cortex.[14,15] Binding to the perineuronal net (PNN)—an extracellular matrix structure enriched in glycosaminoglycans (GAGs) that tightly enwrap PV+ cells as they mature—is a crucial step.[15,18–20] Thus, cortical infusion of exogenous Otx2 protein just after eye opening (but before normal CP onset) accelerates PV+ cell maturation in V1 and prematurely triggers plasticity in mice,[14] whereas CP onset is delayed by extracellular blockade of Otx2 protein.[15] Conversely, PNN removal or reducing Otx2 levels in adulthood reopens a new window of plasticity.[15,16,18] Of therapeutic relevance,[2,4] the latter manipulations successfully restore vision to amblyopic mice.[15,16]

We previously identified a short arginine-rich sugar-binding motif within Otx2 that interacts specifically with disulfated chondroitin sulfate GAG side chains in the PNN.[15] Here, we used a knock-in mouse bearing point mutations in this motif. This allowed us first to determine whether the short peptide sequence is intrinsically needed for PNN-mediated PV+ cell-specific Otx2 localization. Second, we could then test whether this Otx2 mutation would have a global impact beyond the visual system by analyzing its effect across modalities. Indeed, we found altered PV+ cell maturation and delayed CP timing not only for amblyopic effects in V1, but also for tonotopic map plasticity and acoustic preference behavior in primary auditory (A1) and medial prefrontal cortex (mPFC), respectively. In turn, PNN components remained dynamic well beyond the normal time of CP closure. This mouse model thus reveals a global role for Otx2 in regulating

[1]FM Kirby Neurobiology Center, Department of Neurology, Boston Children's Hospital, Harvard Medical School, Boston, MA, USA; [2]Center for Interdisciplinary Research in Biology (CIRB), CNRS UMR 7241/INSERM U1050, Labex Memolife, Collège de France, Paris, France; [3]Center for Brain Science, Department of Molecular Cellular Biology, Harvard University, Cambridge, MA, USA; [4]Institute of Genetics and Biophysics 'Adriano Buzzati-Traverso', Naples, Italy and [5]IRCCS Neuromed, Pozzilli, Italy. Correspondence: AA Di Nardo, Center for Interdisciplinary Research in Biology, CNRS UMR 7241/INSERM U1050, Labex Memolife, Collège de France, Paris, France or Professor TK Hensch, Center for Brain Science, Department of Molecular Cellular Biology, Harvard University, 52 Oxford Street (NW 347.10), Cambridge, MA 02138, USA.
E-mail: ariel.dinardo@college-de-france.fr or hensch@mcb.harvard.edu
[6]These authors contributed equally to this work.
Received 27 April 2016; revised 21 November 2016; accepted 21 December 2016

CP timing throughout the cortex and confirms the importance of GAG binding in localizing non-cell autonomous Otx2 to PV+ cells.

MATERIALS AND METHODS

Animals

The Otx2-AA mouse line was generated through a knock-in approach, as described previously.[21] In all tests performed, there were no differences between wild-type animals from different litters. All procedures were designed to minimize animal suffering and carried out in accordance with recommendations of the European Directive 86/609 (EEC Council for Animal Protection in Experimental Research and Other Scientific Utilization) and the IACUC committee of Boston Children's Hospital.

Immunohistochemistry

Mice were perfused transcardially with phosphate-buffered saline followed by 4% paraformaldehyde prepared in phosphate-buffered saline. Brains were dissected, post-fixed overnight at 4 °C in 4% paraformaldehyde and immunohistochemistry was performed on free-floating sections (40 µm). Sections were incubated with primary antibodies overnight at 4 °C, intensively washed and further incubated with corresponding Alexa Fluor-conjugated secondary antibodies for 1 h at room temperature. The following primary antibodies were used: anti-Otx2 (mouse monoclonal, in house), anti-cFos (rabbit polyclonal, 1/500, Santa Cruz, Dallas, TX, USA), anti-Cux2 (rabbit polyclonal, 1/200, Sigma, Lyon, France), anti-somatostatin (rat monoclonal, 1/500, Millipore, Fontenay sous Bois, France), anti-calbindin (rabbit polyclonal, 1/200, Millipore), anti-VIP (rabbit polyclonal, 1/200, Genetex, Irvine, CA, USA), anti-calretinin (rabbit polyclonal, 1/200, Swant, Marly, Switzerland) and anti-PV (rabbit polyclonal, 1/500, Swant). Secondary antibodies were used as follows: anti-mouse Alexa Fluor 488 (1/2000, Molecular Probes, Illkirch, France) and anti-rabbit Alexa Fluor 546 (1/2000, Molecular Probes).

Biotinylated Wisteria Floribunda Agglutinin (WFA) (1/100, Sigma-Aldrich, St Louis, MO, USA) was used to reveal PNNs and streptavidin-conjugated Alexa Fluor 633 (1/2000, Molecular Probes) was used for its detection. Stained sections were mounted in Fluoromount medium (Southern Biotech, Birmingham, AL, USA) and images were acquired with a Leica SP5 confocal microscope (Nanterre, France). Staining intensity analyses and cell counting were then carried out using ImageJ software (NIH, Bethesda, MD, USA). In brief, a threshold was applied in order to subtract background signal. Size and circularity filters were used to remove false-positive structures, whereas 4,6-diamidino-2-phenylindole counterstain was used to visually confirm that the analyzed structures were cells. For extracellular WFA staining, the mean intensity of the entire image was analyzed in order to quantify staining on both the cell body and its projections. Colocalizations of different antibodies stains were quantified manually.

Monocular deprivation

Mice were anesthetized by isoflurane and the left eyelid was sutured shut before returning to normal housing cage with littermates.[5] The suture was monitored daily for 4 days to ensure complete closure.

Visual evoked potential recording

Mice were anesthetized using a mixture of nembutal/chlorprothixene/dexamethasone, and a tracheotomy performed to provide constant O_2 supply and isoflurane supplementation (0.5–1%). After exposure of V1 via craniotomy, a high-resistant tungsten electrode was inserted to 300–400 µm beneath the pial surface to cortical layer IV (L4). Transient visual evoked potentials (VEPs) in response to abrupt contrast reversal (100%, 1 Hz) of spatial frequency ranging from 0.05 to 0.5 cycles per degree were band-pass filtered (0.1–100 Hz), amplified and fed to custom computer software where $\geqslant 20$ events were averaged in synchrony with the stimulus contrast reversal. A non-linear regression between VEP amplitude and spatial frequency was plotted, and the visual acuity defined as the spatial frequency at which the regression line reaches zero.

Voltage-sensitive dye imaging of A1 tonotopy

Mouse pups and mothers were placed in a sound-attenuating chamber and passively exposed to 7 kHz tones (100 ms pulses at 5 Hz for 1 s, followed by 2 s of silence, 80 dB sound pressure level) generated by Audacity software (Audacity team, USA).

The brain was sectioned peri-horizontally (600 µm, 15°) to preserve the ventral medial geniculate and its projection to the A1.[22] Thalamocortical brain slices were incubated for at least 90 min in the voltage-sensitive dye, Di-4-ANEPPS (5 µg l^{-1}, D-1199, Invitrogen, Carlsbad, CA, USA). Six sites in the ventral medial geniculate were activated with a glass pipette along the latero-medial axis (5 mA, 1 ms pulse; Iso-Flex, A.M.P.I., Jerusalem Israel; spaced at 100 µm). Fluorescence signals (1 ms frame rate; 512 ms) were imaged from regions of interest (130 × 130 µm) along the rostro-caudal axis of A1 at a fixed distance from a reference (rostral point of hippocampus) and at constant depth from the pia, corresponding to upper L4. Excitation light from a shuttered LED (BrainVision, Tokyo, Japan) was reflected toward the slice. Emitted fluorescence was imaged using a MiCam Ultima CMOS-based camera (SciMedia, Costa Mesa, CA, USA) and fluorescence change normalized to resting fluorescence (ΔF/F0). Peak amplitude was defined as the maximum response across all L4 locations averaged over ten trials (MiCam Ultima analysis software, SciMedia, Costa Mesa, CA, USA). Individual time course traces were exported to Igor Pro (WaveMetrics, Portland, OR, USA) for analysis.

Acoustic preference behavior and open field task

Mice were assessed for acoustic preference, first naively then again after music exposure (2 weeks, Symphony No. 1 in C major, Op. 21, by Ludwig van Beethoven). The acoustic preference test[23] was conducted using a Phenotyper 4500 (Noldus Information Technology, Leesburg, VA, USA), a 45 cm (width) × 45 cm (depth) × 45 cm (height) open arena with clear plastic walls viewed by means of a ceiling-mounted video camera and infrared lights and filters. Two diagonally opposing corners of the Phenotyper 4500 were chosen randomly and furnished with red, opaque plastic shelters bearing a side entrance. A small loudspeaker (1.6 cm diameter × 1 cm height) was installed on the ceiling of each shelter (6 cm high), where nesting and bedding materials were provided at the bottom (Figure 3d). To minimize ambient noise interference, the entire test setup was placed in an anechoic sound isolation chamber (inner dimensions: 55 cm (width) × 49 cm (depth) × 66 cm (height); Industrial Acoustics Company (Bronx, NY, USA)) with an ambient light source (8 W).

Each test was initiated by placing mice in the center of the arena and monitored for 3-h consecutively. The animals' behavior was recorded by video camera, tracked and analyzed using Ethovision XT software (Noldus Information Technology). Tests were conducted between 0900 and 1700 hours during the light phase to promote mouse dwelling in the shelters. All components of the test setup were wiped clean twice with Clidox solution, followed by 70% ethanol/30% purified water and ddH_2O, and then air-dried between each trial. The positions of shelters and sound playback were randomized on each trial.

To assay preference, time spent in each shelter during the final 30 min was measured. Mice spending most (80%) of their time in open areas within the test arena but outside either shelter were labeled as having made 'no choice' and dropped from further analysis. Preference for silence or for music was calculated, respectively, as (percentage) 100 × (time in silent shelter/total time in both shelters) or 100 × (time in music shelter/total time in both shelters). Animals spending 75% or more of their time in silent shelter were classified as preferring 'silence', whereas those spending 75% or more in music shelter were classified as 'music' and the remainder as 'equal'. Overall, activity in the open field was measured by center dwell time, distance (cm) moved, and the number of center crossings during the first 30 min via video recording and quantification with Ethovision XT software.

Reverse transcription and quantitative PCR

Cortical tissue micro-dissection was carried out as previously described.[24] In brief, dissected tissues were snap frozen in liquid nitrogen, lysed in trizol reagent at 4 °C and RNA extracted using the RNeasy Micro extraction kit (Qiagen, Courtaboeuf, France). Genomic DNA was digested before elution from column. Isolated RNA was then subjected to quantification and purity check (Nanodrop, Palaiseau, France). Equivalent amounts of RNA were subjected to reverse transcription using a high capacity RNA-to-complementary DNA kit (Applied Biosystems, Waltham, MA, USA) to obtain complementary DNA. Quantitative PCR reactions were set up using Taqman Universal Master Mix (Applied Biosystems) and Taqman probes used as follows: Aggrecan, Brevican, Neurocan, Versican, TenascinR, Hapln1, Hapln4, Mme, Adamts4, Adamts8, Adamts15, MMP15, MMP24, Has1, Has2, Has3, CSGalNAcT1, C6ST-1, Ptprz1, Reln, PTPσ, RTN4R, SST, Calb1, Calb2, Htr3a and Gapdh. All probes were 6-carboxyfluorescein-

conjugated except Gapdh, which was conjugated with VIC (proprietary to Life Technologies, Woburn, MA, USA) serving as internal control. PCR reactions were performed on a StepOnePlus Real-Time PCR system (Applied Biosystems) in 96-well plates using a standard curve protocol. To quantify gene expression, standard curves loaded with known amount of complementary DNA were used for each probe. All results were internally normalized to Gapdh expression, then calculated with reference to standard curves by the StepOne Real-Time PCR systems software v2.1 (Applied Biosystems).

Statistical analysis

Wilcoxon signed-rank tests were used to compare before/after measures. Mann–Whitney *U*-tests (for data with non-normal distributions) and Student's *t*-tests (for data with Gaussian distributions) were conducted for comparisons of two independent samples. Chi-square tests were performed for group comparisons in acoustic preference tests. Two-way analysis of variance tests were used for analyzing (voltage-sensitive dye imaging) results across cortical L4 locations and ventral medial geniculate stimulus sites. Statistical analyses were performed using SYSTAT 13 (Cranes Software International, Karnataka, India) or GraphPad Prism 6 (La Jolla, CA, USA).

RESULTS

Altered Otx2 protein localization and delayed PV and PNN expression in Otx2$^{+/AA}$ mouse V1

An arginine-rich GAG-binding motif spans the junction between the N-terminal and homeodomain in Otx2 (Figure 1a). This motif can be weakened through an R36A and K37A double mutation (RK to AA) that reduces affinity for GAGs,[15] which led us to construct an Otx2-AA knock-in mouse line (both heterozygous *Otx2*$^{+/AA}$ and homozygous *Otx2*$^{AA/AA}$ mice).[21] Our previous study had revealed a gene dosage-dependent impairment of retinal structure,[21] as confirmed here by loss of visual acuity only in the Otx2-AA homozygous mutants (Supplementary Figures S1a and b). We therefore focused on the Otx2-AA heterozygous animals.

In layer IV of juvenile *Otx2*$^{+/AA}$ mouse V1, Otx2 protein levels were lower within each recipient cell compared with that of wild-type (WT) littermates, whereas the number of PNN-bearing cells (positive for WFA staining), containing Otx2 did not change (Supplementary Figure S1e). Notably, Otx2 failed to accumulate markedly in PNN-bearing cells during juvenile development up to P100 (Figure 1c). PNNs typically intensify during this period in WT mice, which is thought to consolidate plastic changes and provide a molecular 'brake' on CP closure.[1,18] Concomitantly over this age range, Otx2 protein in WT mice increased significantly in WFA+ cells (Figure 1c), consistent with a positive feedback model that maturing PNNs condense to permit higher levels of Otx2 protein to accumulate.[15]

Instead, we found significantly increased accumulation of Otx2 protein in non-PNN-bearing cells (negative for WFA) of *Otx2*$^{+/AA}$ visual cortex (Figures 1b and e). This ectopic localization led to ~20% increase in the total number of Otx2+ cells (Figure 1d). In addition, these changes were more pronounced in Otx2-AA homozygous mutants indicating a dose-dependent effect (Supplementary Figures S1c-d). We further studied the identity of these cells that ectopically accumulated Otx2, and found that in

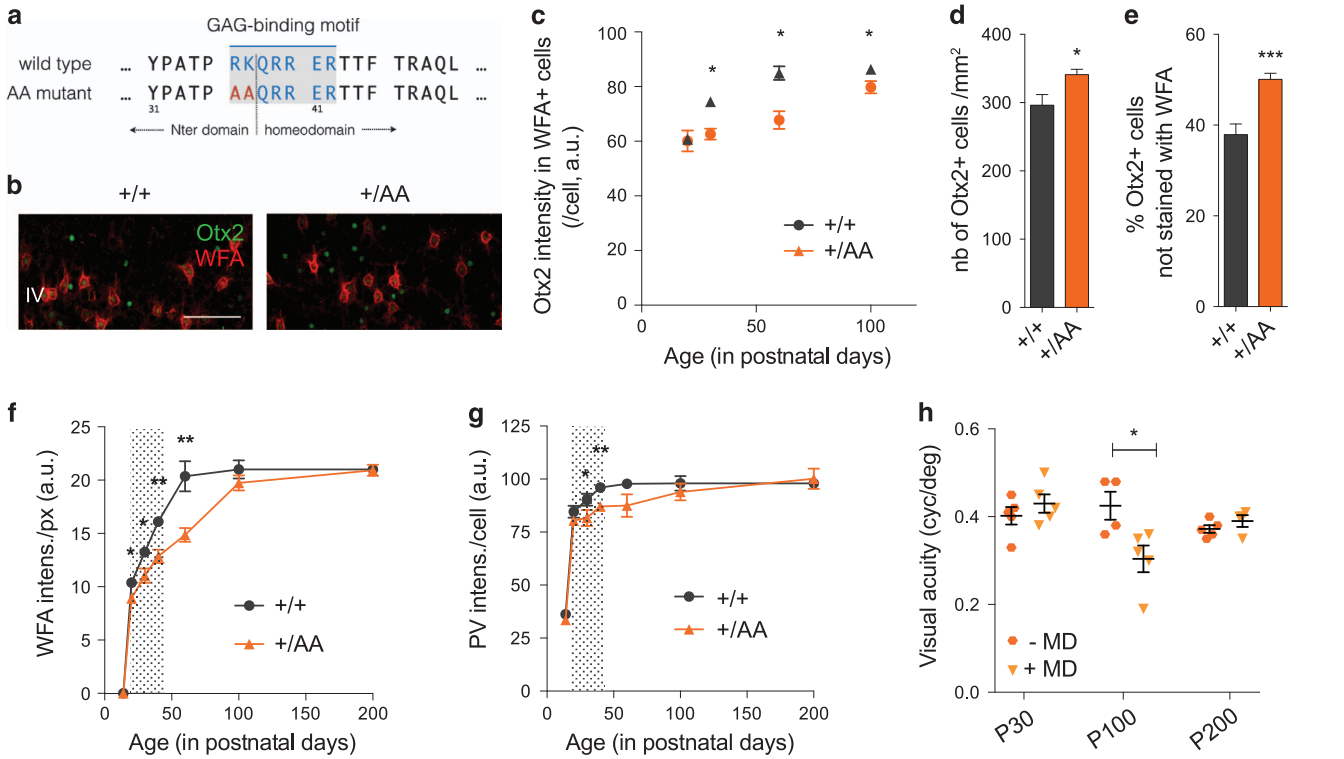

Figure 1. Delayed PV+ cell maturation and visual cortical plasticity in *Otx2*$^{+/AA}$ mice. (**a**) A GAG-binding motif is found between the N-terminal (Nter) and the homeodomain of Otx2. The 'RK' doublet is mutated to 'AA' in the resulting AA mutant. (**b**) Representative images of Wisteria Floribunda Agglutinin (WFA) (staining for perineuronal net (PNN)) and Otx2 co-labeling in primary visual cortex (V1) layer IV (L4) at P30 (scale bar: 100 μm), comparing +/+ (wild-type (WT)) and +/AA (heterozygous *Otx2*$^{+/AA}$). (**c-e**) Quantification of Otx2 immunostaining intensity (arbitrary unit, a.u.) in V1 L4 WFA+ cells from P20 to P100 (**c**, $N = 3–5$ mice per group), total number of Otx2+ cells at P60 (**d**, $N = 9–12$ mice per group) and percentage of Otx2+ cells not stained with WFA at P60 (**e**, $N = 9–12$ mice per group). (**f, g**) WFA staining intensity (a.u.) per pixel (**f**) and parvalbumin (PV) staining intensity (a.u.) per cell (**g**) in V1 L4, quantified from P14 to P200 ($N = 3–10$ mice per group). Shaded area indicates WT ocular dominance critical period. (**h**) Visual acuity measurements of *Otx2*$^{+/AA}$ at P30, P100 and P200, with or without short-term (4-day) monocular deprivation (MD; $N = 4–5$ mice per group). (All values: mean ± s.e.m.; *t*-test; $^*P < 0.05$, $^{**}P < 0.01$, $^{***}P < 0.001$).

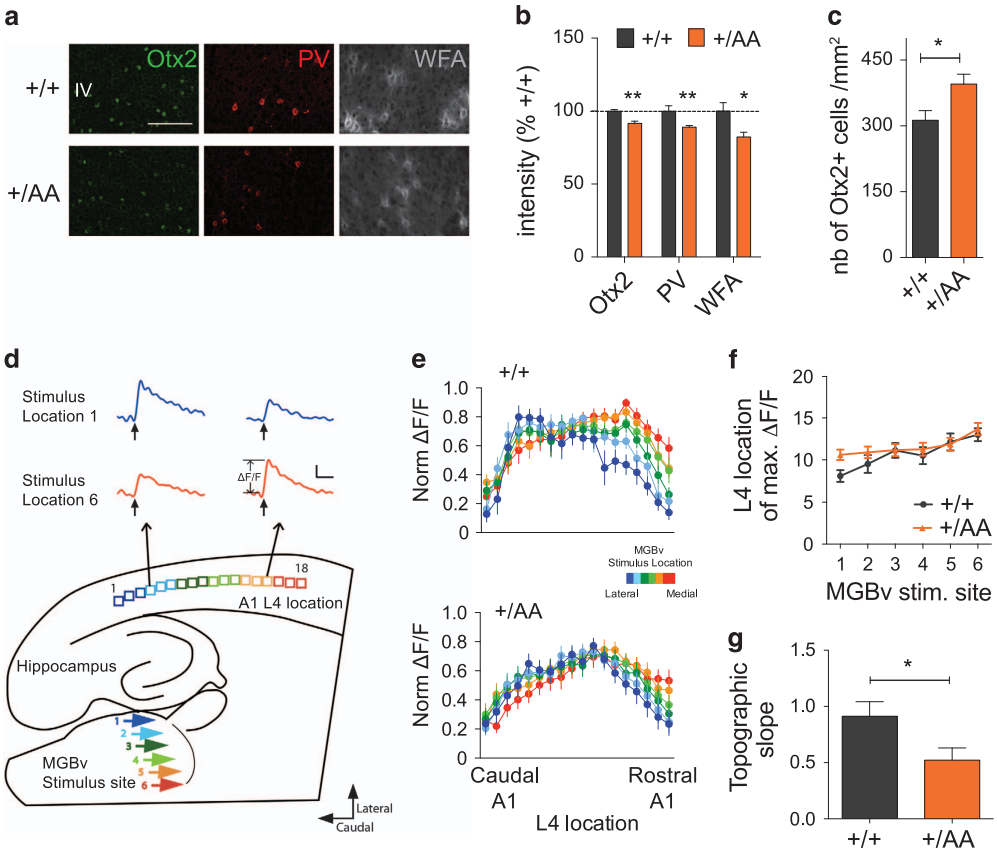

Figure 2. Delayed auditory plasticity in *Otx2*$^{+/AA}$ mice. (**a**) Representative images of Otx2, parvalbumin (PV) and Wisteria Floribunda Agglutinin (WFA) staining in primary auditory cortex (A1) layer IV (L4) at P20 (scale bar: 100 μm). (**b, c**) Staining intensity of Otx2, PV and WFA (**b**, $N = 4–7$ mice per group) and number of Otx2+ cells (**c**, $N = 5–8$ mice per group) in A1 L4 at P20. (**d**) Illustration of thalamocortical brain slice preparation to study auditory plasticity (representative traces from a wild-type (WT) slice, scale bar: 100 ms, 0.05 ΔF/F). (**e**) Normalized (norm.) maximal ΔF/F across L4 loci in response to different ventral medial geniculate body (MGBv) stimulus sites for WT ($N = 13$, $P < 0.0001$ for stimulus location, two-way analysis of variance) and *Otx2*$^{+/AA}$ ($N = 18$, $P = 0.0986$ for stimulus location) mice exposed to a 7 kHz tone between P16 and 20. (**f, g**) Topographic slope calculated from location of maximal Δ*F*/*F* across L4 loci in response to different MGBv stimulus sites 1–6. (All values: mean ± s.e.m.; *t*-test; $*P < 0.05$, $**P < 0.01$).

Otx2$^{+/AA}$ mutants, there was a significant increase in calretinin (CR)+ interneurons colocalizing Otx2, but not in pyramidal cells or other subtypes of inhibitory interneurons (Supplementary Figure S2a). However, mis-localization of Otx2 did not lead to changes in cell numbers or gene expression of these neural markers (Supplementary Figures S2b–c).

We then broadened the longitudinal time window over which we examined WFA and PV staining of V1 in layers IV and above, from P14 to P200 (Figures 1f-g). In *Otx2*$^{+/AA}$ mice, WFA intensity was significantly weaker between P20 and P60 compared with WT littermates. However, its level finally reached that of WT littermates by P100 (Figure 1f). PV staining was similarly lower in *Otx2*$^{+/AA}$ mice before P100 (Figure 1g), with significant differences measured at P30 and P40. Although the intensities for both markers reached a plateau around P60 in WT mice, they did so only after P100 in *Otx2*$^{+/AA}$ mice. Taken together, the RK to AA mutation delayed PNN assembly and PV+ cell maturation, consistent with Otx2 protein mis-localization.

Normal baseline acuity but delayed visual plasticity in Otx2$^{+/AA}$ mice

Both PNN and Otx2 levels reflect postnatal neuronal activity.[14] Given that Otx2 regulates the development of embryonic forebrain[25,26] and eye,[27] reduced accumulation of Otx2-AA protein in the cortex could have been due to compromised retinal activity rather than lowered Otx2 affinity for the PNN. Although heterozygous *Otx2*$^{+/AA}$ mice show no gross developmental defects, homozygous *Otx2*$^{AA/AA}$ mice exhibit microphthalmia and anophthalmia with incomplete (15%) penetrance.[21] This is mirrored by histological and physiological defects found in homozygous *Otx2*$^{AA/AA}$ mice, but not seen in heterozygous *Otx2*$^{+/AA}$ mice.[21] As baseline visual acuity was similar between WT and heterozygous *Otx2*$^{+/AA}$ mice throughout life (Supplementary Figure S1b), we restricted our functional analysis only to these mice for the subsequent study of cortical maturation and plasticity.

To assess the functional consequences of RK to AA mutation in CP timing, a brief 4-day MD was followed by VEP assessment of acuity at P30, P100 and P200 to match the delayed PV+ circuit development in *Otx2*$^{+/AA}$ mice. Strikingly, these mice lost acuity after MD only at P100, but not at P30 or P200 (Figure 1h, Supplementary Figures S3e–g). This time course was shifted as compared with WT mice, which showed typical visual plasticity at P30 but not later[28] (Supplementary Figures S3a–d). Thus, the Otx2 GAG-binding motif is essential for the endogenous maturational trajectory of PV + cells and consequent timing of CP plasticity in V1.

Delayed auditory plasticity in Otx2$^{+/AA}$ mouse A1 and mPFC

We next examined whether Otx2 RK to AA mutation may also affect timing of other CP events.[16] In mice, optimal auditory processing involves thalamocortical refinement in the days following hearing onset. During a brief 3-day window starting

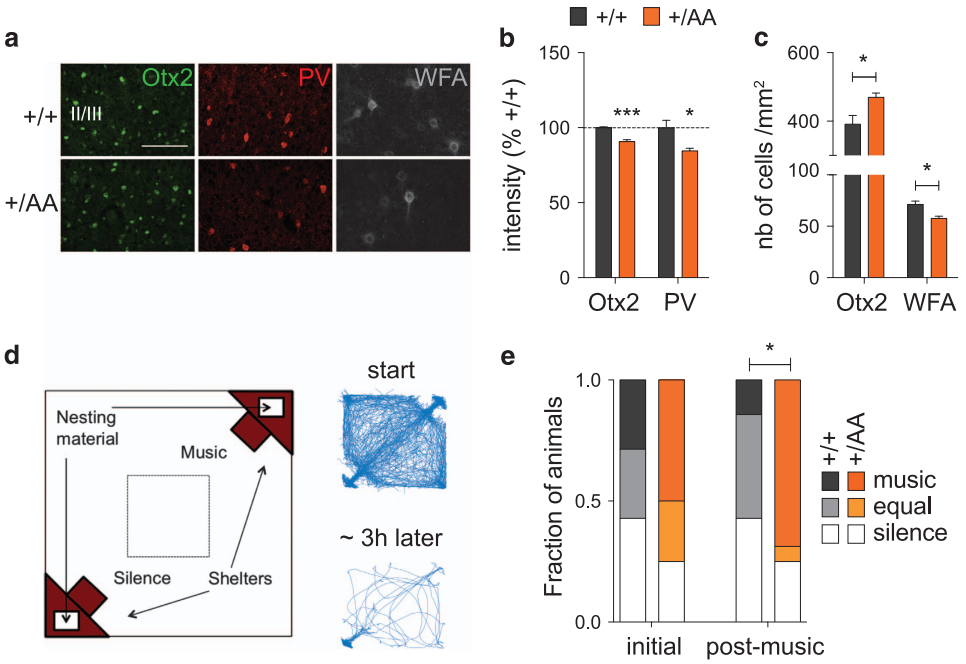

Figure 3. Altered experience-dependent acoustic preference in adult *Otx2*$^{+/AA}$ mice. (**a**) Representative images of Otx2, parvalbumin (PV) and Wisteria Floribunda Agglutinin (WFA) immunostaining in medial prefrontal cortex (mPFC) supragranular layers at P60 (scale bar: 100 μm). (**b**, **c**) Staining intensity of Otx2 and PV (**b**, $N = 4$ mice per group) and number of Otx2+ and WFA+ cells (**c**, $N = 4–5$ mice per group) in supragranular layers of the infra- and pre-limbic regions of mPFC at P60. (**d**) Typical traces of activity of a mouse inside the arena at the start (first 30 min) and at the end (last 30 min of the 3 h experiment) of the acoustic preference behavior assay. (**e**) Adult (P60) mice were passively exposed to music for 2 weeks and tested for acoustic preference. Cumulative frequency distribution of wild-type ($N = 7$) and *Otx2*$^{+/AA}$ mice ($N = 16$) before (initial) and after (post-music) 2-week music exposure. (All values: mean ± s.e.m.; $^{*}P < 0.05$, $^{***}P < 0.001$).

from P12, passive tone rearing can modify response strength and topography in A1.[22] Given the earlier emergence of PV+ cells in A1, it has been hypothesized that they also have a role in auditory CP plasticity.[29] In fact, Otx2 accumulates in PV+ cells of A1 similar to V1.[16] Immunohistochemical analysis in *Otx2*$^{+/AA}$ mice also revealed a delayed PV+ cell maturation and Otx2 protein mis-localization at P20 after the typical auditory CP (Figures 2a–c).

As *Otx2*$^{+/AA}$ mice exhibited normal auditory thresholds as measured by auditory brainstem response (Supplementary Figure S1f), we pursued further functional analyses. Using voltage-sensitive dye imaging in an acute thalamocortical brain slice preparation,[22] we found that late passive tone rearing from P16 to 20 altered the topography in A1 of *Otx2*$^{+/AA}$ mice, at an age when WT littermates were no longer plastic[22] (Figures 2d–g). Thus, targeted accumulation of Otx2 in PV+ cells also has a role in regulating CP timing in A1.

Sequentially after this basic tonotopic plasticity, exposure to more complex acoustic stimuli (such as music) can shape lasting preference behaviors in mice. During a 10-day window starting at P15 (but not in adulthood), the mouse's innate bias for silent shelter can be shifted in favor of music, revealing CP plasticity for this complex behavior.[23] Neurons in the mPFC concurrently develop a biased responsiveness in favor of the acquired music preference.[23] Immunohistochemistry again revealed a delayed PV+ cell maturation and broadly dispersed Otx2 protein in the mPFC of *Otx2*$^{+/AA}$ mice at P60 (Figures 3a–c), suggesting a potential delay in this higher cognitive CP.

Using a nesting paradigm requiring no training and free of confounding olfactory, visual or tactile cues (Figure 3d), we found that music exposure for 2 weeks at P60 successfully reversed the innate preference for silent shelter only in *Otx2*$^{+/AA}$ mice (Figure 3e). Acquisition of preference behavior is related to other limbic functions of mPFC circuits.[23,30] Here too, we found that the delayed acquisition of a music preference in adulthood was linked to anxiolysis. The duration and number of center crossings during the first 30- min exploratory phase in the open field were increased after music exposure (Figures 4a–c). In addition, the *Otx2*$^{+/AA}$ mice showed increased cFos activity in mPFC following music exposure at P60 as compared with WT mice (Figures 4d–f, Supplementary Figure S4), which was seen only if the mice were exposed to music (Supplementary Figures S5a–c). Specifically, the percentage of Otx2+ cells co-stained with cFos was also increased in *Otx2*$^{+/AA}$ mice only after music exposure (Figure 4g, Supplementary Figure S5d), accounting for a subset of cells engaged by the music. Taken together, the same *Otx2*$^{+/AA}$ mice carry a delayed CP plasticity across multiple brain regions.

Persistent turnover of PNN components in Otx2$^{+/AA}$ mouse cortex

To investigate a molecular correlate underlying the shifted plasticity profile in *Otx2*$^{+/AA}$ mice, we examined PNN integrity in further detail. This complex extracellular matrix structure integrates a variety of components,[31] including: (1) core proteins (aggrecan, brevican, neurocan, versican, tenascinR);[32,33] (2) link proteins (Hapln1,4);[34] (3) membrane-bound chondroitin sulfate proteoglycan (CSPG) receptors (PTPσ, RTN4R);[35–37] (4) enzymes responsible for the construction (CSGalNAcT1; Has1,2,3);[32,38] and (5) degradation (Adamts4,8,15; MMP15,24; Mme)[39–41] or modification (C6ST-1, Ptprz1, Reln)[19,32,39] of the PNN. We, therefore, directly compared expression levels in a sensory and prefrontal area across a panel of these 22 PNN-related genes using reverse transcription-quantitative PCR of micro-dissected brain homogenates from WT and *Otx2*$^{+/AA}$ mice.

Remarkably few genes were altered during ectopic plasticity in V1 at P100 (Figure 5a) and PFC at P60 (Figure 5b) of *Otx2*$^{+/AA}$ mice. Notably, core (aggrecan or brevican) and link proteins (Hapln1 or 4) were elevated in both areas. Proteases were also elevated in

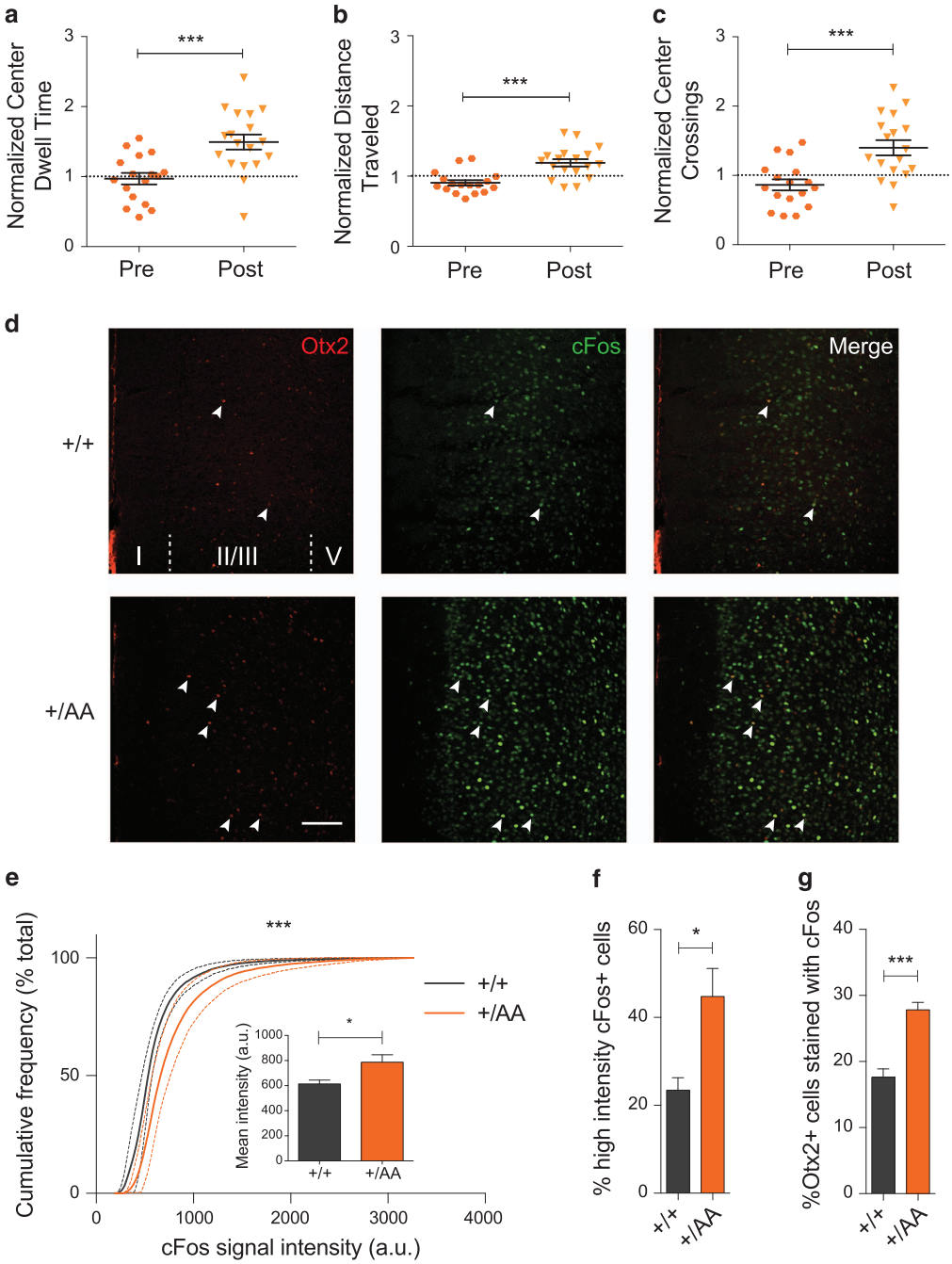

Figure 4. Anxiolysis and recruitment of medial prefrontal cortex (mPFC) circuits following music exposure in *Otx2*$^{+/AA}$ mice. (**a-c**) Open field behavior in the first 30 min reflecting exploratory anxiety are compared before (pre) and after (post) 2-week exposure of *Otx2*$^{+/AA}$ mice to music. Several parameters are compared: (**a**) duration of time spent at the center of the open field, (**b**) total distance traveled in the field and (**c**) number of times crossing the center of the open field. All data are normalized to wild-type (WT) littermates conditions ($N = 17$ mice per genotype). (**d-g**) Immunofluorescence staining of Otx2 and cFos in mPFC reveals circuit activation after 1 h of music exposure. (**d**) Representative images of Otx2 and cFos staining in mPFC at P60 (scale bar: 100 μm, cortical layers I–V are labeled). cFos signal intensity between genotypes is compared under several parameters: (**e**) cumulative frequency plot, (inset) mean intensity (arbitrary unit, a.u.), (**f**) percentage of high intensity cFos+ cells. (**g**) Percentage of Otx2+ cells colocalized with cFos staining (indicated by arrowheads in (**d**) ($N = 5$ mice per genotype). (All values: mean ± s.e.m.; *t*-test in **a-c** and **f-g**, Kolmogorov-Smirnov test in **e**; $^{*}P < 0.05$, $^{***}P < 0.001$).

the PFC, such as Adamts8 and MMP15, whereas the latter was reduced in V1. Region-specific changes were seen for Has2 in V1 and CSPG receptors (PTPσ, RTN4R) in PFC. No other PNN-related genes were altered significantly by the Otx2 RK to AA mutation. These results suggest a dynamic turnover of particular PNN components across brain regions because of Otx2 mis-localization, consistent with delayed plasticity reminiscent of the juvenile brain.

Overall, Otx2-AA protein was mis-localized to one class of non-PNN-bearing cell type (Figures 5c and d), the CR+ interneuron identified previously.[14] It is possible that CSPGs not visible by WFA staining enwrap these cells. Nevertheless, the ectopic Otx2 in CR+ cells neither altered CR expression (Figures 5e and f) nor compensated for the depleted PV+ cells, as CP timing was delayed across brain regions.

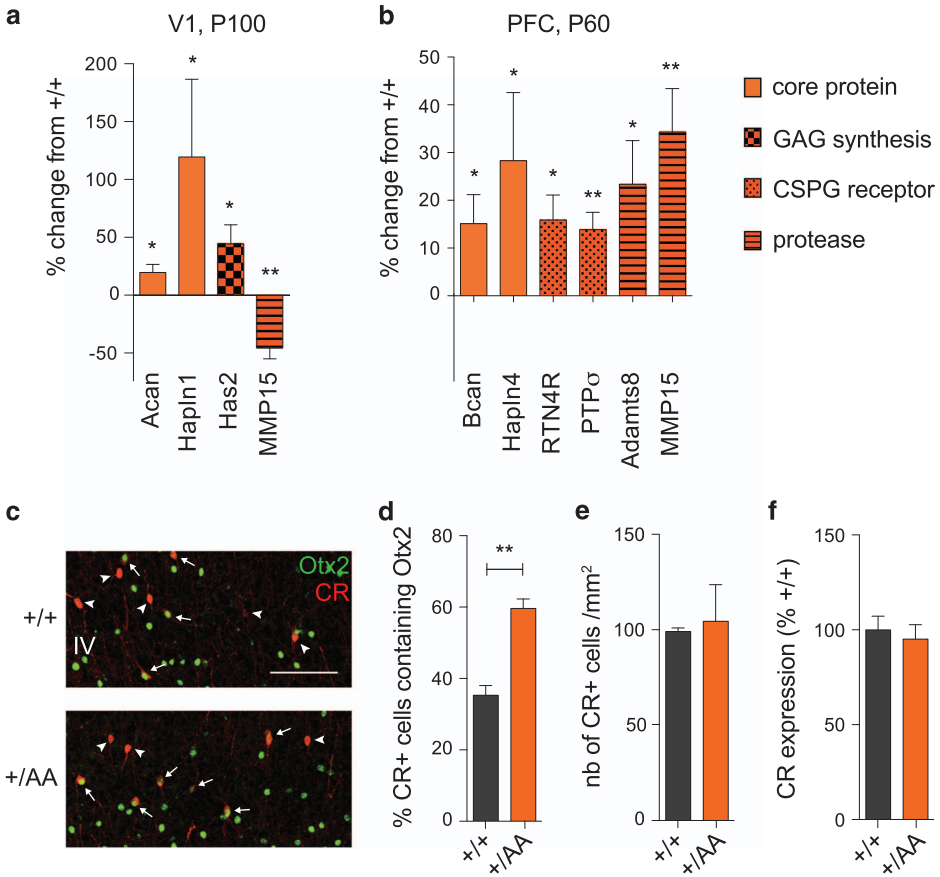

Figure 5. Perineuronal net (PNN) turnover and ectopic Otx2 accumulation in *Otx2*$^{+/AA}$ mice. (**a, b**) PNN genes whose expression is changed between *Otx2*$^{+/AA}$ and wild-type (WT) mice in V1 at P100 (**a**) and in prefrontal cortex (PFC) at P60 (**b**). Results are represented by the percentage change from WT mice ($N = 5$ mice per group). (**c-e**) Ectopic Otx2 accumulation in calretinin (CR)+ cells. (**c**) Representative images of Otx2 and CR co-labeling in V1 layer IV (L4) at P60 (scale bar: 100 μm). (**d**) Percentage of CR+ cells accumulating Otx2 in V1 L4 at P60. (**e**) Total number of CR+ cells in V1 L4 at P60 ($N = 3$ mice per group). (**f**) CR gene expression in V1 ($N = 6$ mice per group). (All values: mean ± s.e.m.; *t*-test; $^{*}P < 0.05$, $^{**}P < 0.01$). Acan, aggrecan; Bcan, brevican; Hapln, hyaluronan and proteoglycan binding link protein; Has, hyaluronan synthase; Adamts, a disintegrin and metalloproteinase with thrombospondin motifs; RTN4R, reticulon 4 receptor; MMP, matrix metalloproteinase; PTPσ, receptor-type protein tyrosine phosphatase σ.

DISCUSSION

In the mature neocortex, PV+ cells are enwrapped by a specific extracellular structure, the PNN. Interestingly, direct modification of this structure[18] or its GAG components[19] extends or reopens windows of cortical plasticity. The PNN environment is enriched in sugar–protein complexes like CSPGs. Infusion of small peptides containing the RK motif found in Otx2 can focally disrupt GAG binding and deplete mature PV+ cells of their Otx2 content to reopen CP plasticity in adult V1.[15] However, this motif may not be unique to Otx2, and PNNs are known to bind a variety of other growth factors, chemokines and axon guidance molecules.[29]

Here, we provide genetic evidence that disrupting the essential GAG-binding motif within endogenous Otx2 alone leads to its mis-localization and attenuates its accumulation in PV+ cells. Although we cannot rule out some role for elevated Otx2 specifically in CR+ cells, none has been identified to date for CP brain plasticity. Instead, we have previously proposed a two-threshold model in which Otx2 controls both the opening and closure of a visual CP through a PV+ cell-positive feedback loop.[16,42] In brief, a nascent PNN surrounding PV+ cells attracts Otx2, which in turn promotes further maturation of the PNN. Our analysis of the Otx2-AA mice supports this model and extends it across multiple brain regions.

Attenuated accumulation (~20% decrease) of Otx2 protein in PV+ cells of V1, A1 and mPFC was sufficient to delay PNN and PV expression and alter CP timing. Instead, development of visual acuity *per se* was normal in V1 of *Otx2*$^{+/AA}$ mice despite having an altered CP, consistent with these features being dissociable.[28] Recently, PV+ cell-intrinsic *Clock* signaling was found to contribute to CP onset,[43] suggesting that once internalized, Otx2 interacts with such mechanisms to fine-tune CP timing. Conversely, plasticity offset is not simply revealed by the structural presence of PNNs, as V1 remained functionally plastic in *Otx2*$^{+/AA}$ mice at P100 although WFA, PV and Otx2 staining intensity levels were near WT. Rather, the biochemical PNN composition was still found to be dynamic. Ultimately, Otx2 may serve as a 'master key' so that other molecules could bind to the emerging net, like NARP,[44] Sema3A[45] and metallopeptidases,[39] which together impact PV+ cell physiology to control plasticity.

At a molecular level, Otx2 signaling was found to regulate PNN core, link and proteolytic proteins known to be produced by PV+ cells,[32,39,46] including Aggrecan, Hapln1/4 and Adamts8. The role of link protein in stabilizing the interaction between aggrecan, versican and hyaluronan to form aggregates is well established.[34] These genes typically follow a downward trajectory throughout development, suggesting a reduced turnover of these components upon PNN consolidation by internalized Otx2. Indeed, increased expression of PNN-associated genes was observed in *Otx2*$^{+/AA}$ mice in both V1 at P100 and mPFC at P60 when plasticity

levels were high. Elevated PTPσ and RTN4R in the PFC of *Otx2*$^{+/AA}$ mice at P60 further suggest CSPG receptor compensation for the loss of their ligands. Notably, C6ST-1 (a determinant of immature sulfation patterns in the PNN related to the open CP in juvenile V1)[19] was unaffected. Ultrastructural and functional dynamics of PNNs after Otx2 mis-localization observed here could be pursued by novel imaging techniques in the future.[47]

Our genetic model reveals that non-cell autonomous Otx2 regulates plasticity broadly across cortical modalities. In *Otx2*$^{+/AA}$mice, PV+ cell maturation was delayed throughout the neocortex and ectopic windows of cortical plasticity arose in occipital, parietal and frontal areas, including A1 and mPFC. This is consistent with a global source of Otx2 coordinating CP timing across brain regions. We previously identified the choroid plexus as one such central Otx2 source.[16] Whether misaligned CP trajectories across brain regions give rise to cognitive consequences will be of great interest. For example, Otx2 signaling may orchestrate complex behaviors reflecting the interplay of multiple sequential CP, such as language[48] and many mental disorders.[49]

Disrupted Otx2 signaling and its consequences may in fact be a hallmark of psychiatric and intellectual disorders.[6,13,50] Multisensory integration in the insular cortex is compromised along with PV+ circuits and their PNNs in mouse models of autism spectrum disorders.[51] PNN density is low in the amygdala, entorhinal and prefrontal cortices of schizophrenia patients[52–54] and high in the motor cortex of patients with Rett Syndrome.[55,56] Weakened PV+ circuits in the mPFC cause deficits in social behavior[57] and behavioral aspects of schizophrenia in both mouse models[58] and patients.[58–61] Gene expression in the choroid plexus is altered in major depressive disorders,[62] and deficits in circadian genes,[63] as well as *Otx2* polymorphisms[17] are associated with bipolar disorders.

One common hub of impairment in these illnesses is elevated oxidative stress,[11] which may normally be buffered by homeoproteins,[64] like Otx2, and *Clock* genes[43] in PV+ cells. This suggests potential therapeutic strategies for preserving or restoring PV+ cell function. Moreover, extending CP plasticity in the mPFC of *Otx2*$^{+/AA}$ mice enabled music to reduce anxiety in adulthood (Figure 4). Potential beneficial effects of judiciously manipulated brain plasticity paired with behavioral therapies[65] may then be promising avenues for psychiatric disorders.

CONFLICT OF INTEREST

The authors declare no conflict of interest.

ACKNOWLEDGMENTS

We thank M Nakamura for mouse maintenance; and support from NIH (1P50MH094271 and 1R01MH104488 to TKH), the Italian Association for Cancer Research (AIRC) (grant IG2013 N° 14152 to AS) and Fondation Bettencourt Schueller, ERC Advanced Grant HOMEOSIGN n° 339379 and ANR (ANR-11-BLAN-069467) (to AP). HHCL and ZY were further supported, respectively, by a post-doctoral fellowship from the Croucher Foundation (Hong Kong) and a Julius B Richmond predoctoral fellowship.

REFERENCES

1 Hensch TK. Critical period plasticity in local cortical circuits. *Nat Rev Neurosci* 2005; **6**: 877–888.
2 Hubel DH, Wiesel TN. The period of susceptibility to the physiological effects of unilateral eye closure in kittens. *J Physiol* 1970; **206**: 419–436.
3 Wang BS, Sarnaik R, Cang J. Critical period plasticity matches binocular orientation preference in the visual cortex. *Neuron* 2010; **65**: 246–256.
4 Sanke RF. Amblyopia. *Am Fam Physician* 1988; **37**: 275–278.
5 Fagiolini M, Hensch TK. Inhibitory threshold for critical-period activation in primary visual cortex. *Nature* 2000; **404**: 183–186.
6 Gogolla N, Leblanc JJ, Quast KB, Sudhof TC, Fagiolini M, Hensch TK. Common circuit defect of excitatory-inhibitory balance in mouse models of autism. *J Neurodev Disord* 2009; **1**: 172–181.
7 Lewis DA, Curley AA, Glausier JR, Volk DW. Cortical parvalbumin interneurons and cognitive dysfunction in schizophrenia. *Trends Neurosci* 2012; **35**: 57–67.
8 Kimoto S, Bazmi HH, Lewis DA. Lower expression of glutamic acid decarboxylase 67 in the prefrontal cortex in schizophrenia: contribution of altered regulation by Zif268. *Am J Psychiatry* 2014; **171**: 969–978.
9 Uchida T, Furukawa T, Iwata S, Yanagawa Y, Fukuda A. Selective loss of parvalbumin-positive GABAergic interneurons in the cerebral cortex of maternally stressed Gad1-heterozygous mouse offspring. *Transl Psychiatry* 2014; **4**: e371.
10 Failor S, Nguyen V, Darcy DP, Cang J, Wendland MF, Stryker MP *et al.* Neonatal cerebral hypoxia-ischemia impairs plasticity in rat visual cortex. *J Neurosci* 2010; **30**: 81–92.
11 Do KQ, Cuenod M, Hensch TK. Targeting oxidative stress and aberrant critical period plasticity in the developmental trajectory to schizophrenia. *Schizophrenia Bull* 2015; **41**: 835–846.
12 LeBlanc JJ, Fagiolini M. Autism: a "critical period" disorder? *Neural Plast* 2011; **2011**: 921680.
13 Le Magueresse C, Monyer H. GABAergic interneurons shape the functional maturation of the cortex. *Neuron* 2013; **77**: 388–405.
14 Sugiyama S, Di Nardo AA, Aizawa S, Matsuo I, Volovitch M, Prochiantz A *et al.* Experience-dependent transfer of Otx2 homeoprotein into the visual cortex activates postnatal plasticity. *Cell* 2008; **134**: 508–520.
15 Beurdeley M, Spatazza J, Lee HH, Sugiyama S, Bernard C, Di Nardo AA *et al.* Otx2 binding to perineuronal nets persistently regulates plasticity in the mature visual cortex. *J Neurosci* 2012; **32**: 9429–9437.
16 Spatazza J, Lee HH, Di Nardo AA, Tibaldi L, Joliot A, Hensch TK *et al.* Choroid-plexus-derived Otx2 homeoprotein constrains adult cortical plasticity. *Cell Rep* 2013; **3**: 1815–1823.
17 Sabunciyan S, Yolken R, Ragan CM, Potash JB, Nimgaonkar VL, Dickerson F *et al.* Polymorphisms in the homeobox gene OTX2 may be a risk factor for bipolar disorder. *Am J Med Genet B Neuropsychiatric Genet* 2007; **144B**: 1083–1086.
18 Pizzorusso T, Medini P, Berardi N, Chierzi S, Fawcett JW, Maffei L. Reactivation of ocular dominance plasticity in the adult visual cortex. *Science* 2002; **298**: 1248–1251.
19 Miyata S, Komatsu Y, Yoshimura Y, Taya C, Kitagawa H. Persistent cortical plasticity by upregulation of chondroitin 6-sulfation. *Nat Neurosci* 2012; **15**: S411–S412.
20 Bernard C, Prochiantz A. Otx2-PNN interaction to regulate cortical plasticity. *Neural Plasticity* 2016; **2016**: 7931693.
21 Bernard C, Kim HT, Torero Ibad R, Lee EJ, Simonutti M, Picaud S *et al.* Graded Otx2 activities demonstrate dose-sensitive eye and retina phenotypes. *Hum Mol Genet* 2014; **23**: 1742–1753.
22 Barkat TR, Polley DB, Hensch TK. A critical period for auditory thalamocortical connectivity. *Nat Neurosci* 2011; **14**: 1189–1194.
23 Yang EJ, Lin EW, Hensch TK. Critical period for acoustic preference in mice. *Proc Natl Acad Sci USA* 2012; **109**(Suppl 2): 17213–17220.
24 Saxena A, Wagatsuma A, Noro Y, Kuji T, Asaka-Oba A, Watahiki A *et al.* Trehalose-enhanced isolation of neuronal sub-types from adult mouse brain. *BioTechniques* 2012; **52**: 381–385.
25 Acampora D, Di Giovannantonio LG, Di Salvio M, Mancuso P, Simeone A. Selective inactivation of Otx2 mRNA isoforms reveals isoform-specific requirement for visceral endoderm anteriorization and head morphogenesis and highlights cell diversity in the visceral endoderm. *Mech Dev* 2009; **126**: 882–897.
26 Acampora D, Mazan S, Lallemand Y, Avantaggiato V, Maury M, Simeone A *et al.* Forebrain and midbrain regions are deleted in Otx2-/- mutants due to a defective anterior neuroectoderm specification during gastrulation. *Development* 1995; **121**: 3279–3290.
27 Nishida A, Furukawa A, Koike C, Tano Y, Aizawa S, Matsuo I *et al.* Otx2 homeobox gene controls retinal photoreceptor cell fate and pineal gland development. *Nat Neurosci* 2003; **6**: 1255–1263.
28 Kang E, Durand S, LeBlanc JJ, Hensch TK, Chen C, Fagiolini M. Visual acuity development and plasticity in the absence of sensory experience. *J Neurosci* 2013; **33**: 17789–17796.
29 Takesian AE, Hensch TK. Balancing plasticity/stability across brain development. *Prog Brain Res* 2013; **207**: 3–34.
30 Garvert MM, Moutoussis M, Kurth-Nelson Z, Behrens TE, Dolan RJ. Learning-induced plasticity in medial prefrontal cortex predicts preference malleability. *Neuron* 2015; **85**: 418–428.
31 Wang D, Fawcett J. The perineuronal net and the control of CNS plasticity. *Cell Tissue Res* 2012; **349**: 147–160.
32 Carulli D, Pizzorusso T, Kwok JC, Putignano E, Poli A, Forostyak S *et al.* Animals lacking link protein have attenuated perineuronal nets and persistent plasticity *Brain* 2010; 133(Pt 8): 2331–2347.
33 Morawski M, Filippov M, Tzinia A, Tsilibary E, Vargova L. ECM in brain aging and dementia. *Prog Brain Res* 2014; **214**: 207–227.

34 Oohashi T, Edamatsu M, Bekku Y, Carulli D. The hyaluronan and proteoglycan link proteins: organizers of the brain extracellular matrix and key molecules for neuronal function and plasticity. *Exp Neurol* 2015; **274**(Pt B): 134–144.
35 Shen Y, Tenney AP, Busch SA, Horn KP, Cuascut FX, Liu K *et al.* PTPsigma is a receptor for chondroitin sulfate proteoglycan, an inhibitor of neural regeneration. *Science* 2009; **326**: 592–596.
36 Dickendesher TL, Baldwin KT, Mironova YA, Koriyama Y, Raiker SJ, Askew KL *et al.* NgR1 and NgR3 are receptors for chondroitin sulfate proteoglycans. *Nat Neurosci* 2012; **15**: 703–712.
37 Stephany CE, Chan LL, Parivash SN, Dorton HM, Piechowicz M, Qiu S *et al.* Plasticity of binocularity and visual acuity are differentially limited by nogo receptor. *J Neurosci* 2014; **34**: 11631–11640.
38 Sato T, Kudo T, Ikehara Y, Ogawa H, Hirano T, Kiyohara K *et al.* Chondroitin sulfate N-acetylgalactosaminyltransferase 1 is necessary for normal endochondral ossification and aggrecan metabolism. *J Biol Chem* 2011; **286**: 5803–5812.
39 Rossier J, Bernard A, Cabungcal JH, Perrenoud Q, Savoye A, Gallopin T *et al.* Cortical fast-spiking parvalbumin interneurons enwrapped in the perineuronal net express the metallopeptidases Adamts8, Adamts15 and Neprilysin. *Mol Psychiatry* 2015; **20**: 154–161.
40 Valenzuela JC, Heise C, Franken G, Singh J, Schweitzer B, Seidenbecher CI *et al.* Hyaluronan-based extracellular matrix under conditions of homeostatic plasticity. *Philos Trans R Soc Lond B Biol Sci* 2014; **369**: 20130606.
41 Zeisel A, Munoz-Manchado AB, Codeluppi S, Lonnerberg P, La Manno G, Jureus A *et al.* Brain structure. Cell types in the mouse cortex and hippocampus revealed by single-cell RNA-seq. *Science* 2015; **347**: 1138–1142.
42 Prochiantz A, Di Nardo AA. Homeoprotein signaling in the developing and adult nervous system. *Neuron* 2015; **85**: 911–925.
43 Kobayashi Y, Ye Z, Hensch TK. Clock genes control cortical critical period timing. *Neuron* 2015; **86**: 264–275.
44 Gu Y, Huang S, Chang MC, Worley P, Kirkwood A, Quinlan EM. Obligatory role for the immediate early gene NARP in critical period plasticity. *Neuron* 2013; **79**: 335–346.
45 Vo T, Carulli D, Ehlert EM, Kwok JC, Dick G, Mecollari V *et al.* The chemorepulsive axon guidance protein semaphorin3A is a constituent of perineuronal nets in the adult rodent brain. *Mol Cell Neurosci* 2013; **56**: 186–200.
46 Giamanco KA, Matthews RT. Deconstructing the perineuronal net: cellular contributions and molecular composition of the neuronal extracellular matrix. *Neuroscience* 2012; **218**: 367–384.
47 Tsien RY. Very long-term memories may be stored in the pattern of holes in the perineuronal net. *Proc Natl Acad Sci USA* 2013; **110**: 12456–12461.
48 Werker JF, Hensch TK. Critical periods in speech perception: new directions. *Annu Rev Psychol* 2015; **66**: 173–196.
49 Meredith RM, Dawitz J, Kramvis I. Sensitive time-windows for susceptibility in neurodevelopmental disorders. *Trends Neurosci* 2012; **35**: 335–344.
50 Maeda N. Proteoglycans and neuronal migration in the cerebral cortex during development and disease. *Front Neurosci* 2015; **9**: 98.
51 Gogolla N, Takesian AE, Feng G, Fagiolini M, Hensch TK. Sensory integration in mouse insular cortex reflects GABA circuit maturation. *Neuron* 2014; **83**: 894–905.
52 Berretta S, Pantazopoulos H, Markota M, Brown C, Batzianouli ET. Losing the sugar coating: potential impact of perineuronal net abnormalities on interneurons in schizophrenia. *Schizophr Res* 2015; **167**: 18–27.
53 Mauney SA, Athanas KM, Pantazopoulos H, Shaskan N, Passeri E, Berretta S *et al.* Developmental pattern of perineuronal nets in the human prefrontal cortex and their deficit in schizophrenia. *Biol Psychiatry* 2013; **74**: 427–435.
54 Pantazopoulos H, Woo TU, Lim MP, Lange N, Berretta S. Extracellular matrix-glial abnormalities in the amygdala and entorhinal cortex of subjects diagnosed with schizophrenia. *Arch Gen Psychiatry* 2010; **67**: 155–166.
55 Krishnan K, Wang BS, Lu J, Wang L, Maffei A, Cang J, Huang ZJ. MeCP2 regulates the timing of critical period plasticity that shapes functional connectivity in primary visual cortex. *Proc Natl Acad Sci USA* 2015; **112**: E4782–E4791.
56 Belichenko PV, Hagberg B, Dahlstrom A. Morphological study of neocortical areas in Rett syndrome. *Acta Neuropathol* 1997; **93**: 50–61.
57 Yizhar O, Fenno LE, Prigge M, Schneider F, Davidson TJ, O'Shea DJ *et al.* Neocortical excitation/inhibition balance in information processing and social dysfunction. *Nature* 2011; **477**: 171–178.
58 Brown JA, Ramikie TS, Schmidt MJ, Baldi R, Garbett K, Everheart MG *et al.* Inhibition of parvalbumin-expressing interneurons results in complex behavioral changes. *Mol Psychiatry* 2015; **20**: 1499–1507.
59 Akbarian S, Kim JJ, Potkin SG, Hagman JO, Tafazzoli A, Bunney WE Jr. *et al.* Gene expression for glutamic acid decarboxylase is reduced without loss of neurons in prefrontal cortex of schizophrenics. *Arch Gen Psychiatry* 1995; **52**: 258–266.
60 Hashimoto T, Volk DW, Eggan SM, Mirnics K, Pierri JN, Sun Z *et al.* Gene expression deficits in a subclass of GABA neurons in the prefrontal cortex of subjects with schizophrenia. *J Neurosci* 2003; **23**: 6315–6326.
61 Glausier JR, Fish KN, Lewis DA. Altered parvalbumin basket cell inputs in the dorsolateral prefrontal cortex of schizophrenia subjects. *Mol Psychiatry* 2014; **19**: 30–36.
62 Turner CA, Thompson RC, Bunney WE, Schatzberg AF, Barchas JD, Myers RM *et al.* Altered choroid plexus gene expression in major depressive disorder. *Front Hum Neurosci* 2014; **8**: 238.
63 Roybal K, Theobold D, Graham A, DiNieri JA, Russo SJ, Krishnan V *et al.* Mania-like behavior induced by disruption of CLOCK. *Proc Natl Acad Scie USA* 2007; **104**: 6406–6411.
64 Rekaik H, Blaudin de The FX, Fuchs J, Massiani-Beaudoin O, Prochiantz A, Joshi RL. Engrailed homeoprotein protects mesencephalic dopaminergic neurons from oxidative stress. *Cell Rep* 2015; **13**: 242–250.
65 Yinger OS, Gooding L. Music therapy and music medicine for children and adolescents. *Child Adolescent Psychiatric Clin N Am* 2014; **23**: 535–553.

Supplementary Information accompanies the paper on the Molecular Psychiatry website (http://www.nature.com/mp)